Proc. Natl. Acad. Sci. USA
Vol. 85, pp. 7993–7997, November 1988
Biophysics

Structure of the reaction center from *Rhodobacter sphaeroides* R-26 and 2.4.1: Protein–cofactor (bacteriochlorophyll, bacteriopheophytin, and carotenoid) interactions*

(bacterial photosynthesis/membrane protein structure/x-ray diffraction)

T. O. YEATES†, H. KOMIYA†, A. CHIRINO†, D. C. REES†, J. P. ALLEN‡, AND G. FEHER‡§

†University of California, Los Angeles, CA 90024; and ‡University of California at San Diego, La Jolla, CA 92093

Contributed by G. Feher, July 22, 1988

ABSTRACT **The three-dimensional structures of the cofactors and protein subunits of the reaction center (RC) from the carotenoidless mutant strain of *Rhodobacter sphaeroides* R-26 and the wild-type strain 2.4.1 have been determined by x-ray diffraction to resolutions of 2.8 Å and 3.0 Å with *R* values of 24% and 26%, respectively. The bacteriochlorophyll dimer (D), bacteriochlorophyll monomers (B), and bacteriopheophytin monomers (ϕ) form two branches, A and B, that are approximately related by a twofold symmetry axis. The cofactors are located in hydrophobic environments formed by the L and M subunits. Differences in the cofactor–protein interactions between the A and B cofactors, as well as between the corresponding cofactors of *Rb. sphaeroides* and *Rhodopseudomonas viridis* [Michel, H., Epp, O. & Deisenhofer, J. (1986) *EMBO J.* 3, 2445–2451], are delineated. The roles of several structural features in the preferential electron transfer along the A branch are discussed. Two bound detergent molecules of β-octyl glucoside have been located near B_A and B_B. The environment of the carotenoid, C, that is present in RCs from *Rb. sphaeroides* 2.4.1 consists largely of aromatic residues of the M subunit. A role of B_B in the triplet energy transfer from D to C and the reason for the preferential ease of removal of B_B from the RC is proposed.**

The reaction center (RC) is an integral membrane protein–pigment complex that mediates the primary processes of photosynthesis—i.e., the light-induced electron transfer from a donor to a series of acceptors. The RC from the carotenoidless mutant *Rhodobacter sphaeroides* R-26 is composed of three protein subunits L, M, and H, and the following cofactors: a bacteriochlorophyll (Bchl) dimer (D), two Bchl monomers (B), two bacteriopheophytin (Bphe) monomers (ϕ), two ubiquinones (Q), and a nonheme iron (for a review, see ref. 1). The cofactors are organized into two branches, A and B,¶ that are approximately related by a twofold symmetry axis (3). The RC from the wild-type strain 2.4.1 contains an additional cofactor, a carotenoid, C, that is believed to protect the RC against photooxidation damage (for a review, see ref. 4).

The three-dimensional structures of the RC from *Rb. sphaeroides* R-26 and 2.4.1 have been obtained to resolutions of 2.8 Å and 3.0 Å, respectively. In previous papers, we reported the structure of the cofactors (3), protein subunits (5), and the membrane–protein interactions (6) of the RC from *Rb. sphaeroides* R-26. In this paper, we discuss the interactions of the proteins with the cofactors D, B, and ϕ, the carotenoid, C, and the detergent β-octyl glucoside (βOG). The protein interactions involving the quinones and iron will be reported in a subsequent publication (7). The structure of the RC from *Rb. sphaeroides* is compared with that of *Rhodopseudomonas viridis* (8), with special emphasis on the structural features that are believed to be important in the electron transfer process. It should be noted that only the structure of the unexcited state of the RC has been reported (2, 8, 9); conformation changes accompanying the absorption of light and subsequent charge separation have not yet been reported.

EXPERIMENTAL PROCEDURES

RC from *Rb. sphaeroides* R-26. Data collection, processing, and initial refinement of the structure of the RC from *Rb. sphaeroides* R-26 at 2.8 Å resolution has been described (3). Subsequent rebuilding of the atomic structure was facilitated by the use of modified "omit-maps." These are typically calculated by removing all atoms from a specified volume in the unit cell and then using the remaining atoms to phase the Fourier calculation for electron density in that volume (10). This approach tends to minimize bias in the electron density map toward the current atomic model. In the present work, a least-squares refinement of an initial omit-map was implemented. The electron density map was sampled at 144, 96, and 144 grid points along the crystallographic *a*, *b*, and *c* axes, respectively. Electron density values within a specific block of 12 × 12 × 12 grid points were varied, while grid points outside this block were fixed at the electron density of the current model. Values of the electron density within the block were refined by a least-squares calculation to minimize the difference between the magnitudes of observed and calculated structure factors. This procedure was repeated for all 288 blocks in the crystallographic asymmetric unit. An asymmetric unit was reconstructed from the blocks, followed by a least-squares version of solvent flattening. The quality of the resulting electron density maps was significantly improved relative to $(|F_o| - |F_c|)$ or $(2|F_o| - |F_c|)$ maps, which are often used in model building. After adjustments of the cofactors, the residues in the L and M subunits, and the addition of two βOG molecules, the atomic structure was refined to an *R* factor of 24.0%, with the restrained least-squares program of Hendrickson and Konnert (as discussed in ref. 11). The H subunit as published in ref. 5 is currently being refined.

Coordinate errors are estimated to be ≈0.5 Å, as determined from Read's σ_A plot (12), implying an error of ≈0.7 Å for interatomic distances. Accordingly, we identified potential hydrogen-bonding interactions if the donor and acceptor

The publication costs of this article were defrayed in part by page charge payment. This article must therefore be hereby marked "*advertisement*" in accordance with 18 U.S.C. §1734 solely to indicate this fact.

Abbreviations: RC, reaction center; Bchl, bacteriochlorophyll; Bphe, bacteriopheophytin; D, Bchl dimer; B, Bchl monomer; ϕ, Bphe monomer; Q, quinone; βOG, β-octyl glucoside; subscripts A and B, branches A and B.

*This is paper no. 4 in a series. Papers 1, 2, 3, and 5 are refs. 3, 5, 6, and 7, respectively.

§To whom reprint requests should be addressed.

¶The nomenclature used in this work follows ref. 2.

atoms are separated by 2.8–3.5 Å, and the correct angular geometry is maintained. At the resolution of the present work, C, N, and O atoms cannot be distinguished. Hydrogen-bonding restraints were not imposed, although side-chain conformations for residues such as His and Bchl acetyl groups were positioned to optimize potential hydrogen-bonding interactions. Potential hydrogen bonds involving solvent molecules have not yet been incorporated into the structure. Mg–ligand distances are observed to be ≈2.0 Å in well-refined structures. Restraints on these distances were not applied during refinement, but the Mg was restrained to the Bchl plane. Direct Mg–ligand interactions were identified by distances <3.0 Å; however, an out-of-plane position of Mg would allow a larger distance between a residue and the Bchl ring center.

RC from *Rb. sphaeroides* 2.4.1. Crystals of RCs from the wild-type strain *Rb. sphaeroides* 2.4.1 were grown under the same conditions as those from strain R-26. The 2.4.1 crystals have the same space group as the R-26 crystals ($P2_12_12_1$), with similar cell constants (2). Intensity data from crystals of wild-type RC (2.4.1) were collected to 3 Å resolution with a multiwire area detector (13) mounted on a Rigaku RU-200 rotating anode generator. Data were merged with the ROCKS crystallographic computing package (14) to a merging R factor of 14% (with $R = \Sigma|I_i - I_j|/\Sigma|I_i + I_j|$, where the measured intensities I are summed over all symmetry reflections i and j). A total of 23,025 unique reflections (74% of reflections between 8 and 3 Å resolution) with intensity exceeding one standard deviation were merged from 73,313 observations. Small adjustments in the cell constants and orientational parameters necessary to position the R-26 model in the 2.4.1 unit cell were made with a real-space rigid body refinement program (15). The repositioned model was then refined by the restrained least-squares method of Hendrickson and Konnert (11). After an initial refinement, the carotenoid was located in a difference Fourier map between the observed and calculated structure factor amplitudes and built as a polyene chain into the difference density. The model has been refined to an R factor of 26.3% (21% for reflections with intensity exceeding twice the estimated standard deviation), with root-mean-square deviations from standard bond distances and angles of 0.026 Å and 5.5°, respectively.

RESULTS

The $Bchl_2$ Dimer. Two of the Bchls form a dimer with their rings I overlapping. The planes of the tetrapyrroles are nearly parallel, with the normals of the two Bchl rings (calculated using a least-squares planar fit) forming an angle of 8°. The Bchl rings are nearly perpendicular to the membrane plane; the Bchl normals form angles of 88° (D_A) and 85° (D_B) with respect to the membrane normal as defined by the direction of the twofold symmetry axis (6). The angles between the lines joining N_1 and N_3 of each Bchl is ≈140°; this angle optimizes the overlap of ring I. The distance between the pyrrole rings I is ≈3.5 Å, which is larger than that reported for *Rps. viridis* (3.0 Å) (16). This larger separation is consistent with the smaller red shift in *Rb. sphaeroides* of the optical band (865 nm) associated with the dimer (17).

The dimer interacts with the C, D, E, and cd helices of both the L and M subunits (5). Residues from each subunit form a hydrophobic environment enclosing the dimer (see Fig. 1). Near the central Mg atoms are histidines M202 and L173, located on the periplasmic side of the D helices. His M202 is coordinated to the Mg of D_B; in contrast, His L173 is too far (4.0 Å) to coordinate directly the Mg of D_A. His L173 may possibly form a hydrogen bond with His L168; this may stabilize His L173 away from the Mg. In *Rps. viridis*, His M200 and His L173 are reported to coordinate to Mg and also form a hydrogen bond to water (18).

In view of the unexpected differences in His–Mg ligation between *Rb. sphaeroides* and *Rps. viridis*, we checked for possible distortions of the electron density maps due to crystallographic artefacts. The omit-maps used for model building should be relatively free from model bias. In addition, tests with calculated structure factors indicated that the His density was not distorted by the absence of reflections missing from the observed diffraction data. The His L173 ring density was of the appropriate size and shape for an imidazole ring. Accordingly, the electron density maps support the positioning of His L173 away from D_A (and His L153 away from B_A, as discussed below).

The acetyl groups of ring I are approximately in the plane of their respective Bchl in the dimer. Both groups are too far from the Mg of the adjacent Bchl to serve as direct ligands. No hydrogen bonds are observed for the acetyl groups. In *Rps. viridis*, hydrogen bonds were reported between the acetyl groups and His L168 and Tyr M195 (8). His L168 is conserved between species. However, in *Rb. sphaeroides* it may form a hydrogen bond with His L173 but not with the acetyl group of D_A, as discussed above. Tyr M195 of *Rps. viridis* is not a conserved residue; the corresponding residue in *Rb. sphaeroides* is Phe M197, whose side chain cannot form a hydrogen bond.

In *Rb. sphaeroides*, the only hydrogen bond involving the dimer and the protein subunits is between the ring IV carbonyl of the propionic acid group of D_A and Tyr M210. In *Rps. viridis*, two additional possible hydrogen bonds were reported involving ring V groups: the keto carbonyl of D_A with Thr L248 and the ester carbonyl group of D_B with Ser M203 (8). Thr L248 is not conserved and the corresponding residue Met L248 of *Rb. sphaeroides* cannot form a hydrogen bond. Ser M203 is conserved (as M205 in *Rb. sphaeroides*) but forms a hydrogen bond with the backbone nitrogen of M280 rather than D_B.

Several aromatic residues are found in the binding site of the dimer (see Fig. 1*A*). Tyrosine L162 lies approximately midway between the dimer and the proposed site of the cytochrome heme (6). The normal of its aromatic ring makes an angle of ≈60° relative to the dimer normal. This residue is conserved and may be involved in the electron transfer from the cytochrome heme to the dimer. Aromatic residues are positioned between D and ϕ for each branch: Tyr M210 along the A branch and Phe L181 along the B branch (3) (see Fig. 1*A*). This asymmetric arrangement may contribute to the preferential electron transfer from D to ϕ_A (see *Discussion*). A more complete discussion of structural asymmetries will be provided later (19). Most charged residues are at least 10 Å away from the tetrapyrrole rings of D, with the exception of Arg L135, which is 8.0 Å away.

The electron density is well defined for the full length of the phytyl chains for both D_A and D_B. The phytyl tails of both cofactors are in contact with the conjugated ring system of the cofactors B and ϕ on the same branch. Of particular interest for electron transfer are the contacts between the D_A phytyl tail with the acetyl group of ϕ_A and with the acetyl group of B_A. These contacts could facilitate electron transfer between the cofactors.

The Bchl Monomers. Each cofactor branch contains a Bchl monomer. The normals of the planes of the Bchl monomers form angles of 30° (B_A) and 35° (B_B) with respect to the membrane normal. The $B_A(B_B)$ monomers interact with the membrane-spanning helices D of the subunits L(M) and the helices C of M(L) as well as the cd helix of M(L) (see Fig. 2).

The Mg ligation is asymmetric. His M182 coordinates to Mg of B_B, but His L153 probably does not ligand to Mg of B_A (see *Discussion*). Instead, His L153 appears to hydrogen bond to the carbonyl oxygen of L149. In *Rps. viridis*, both His

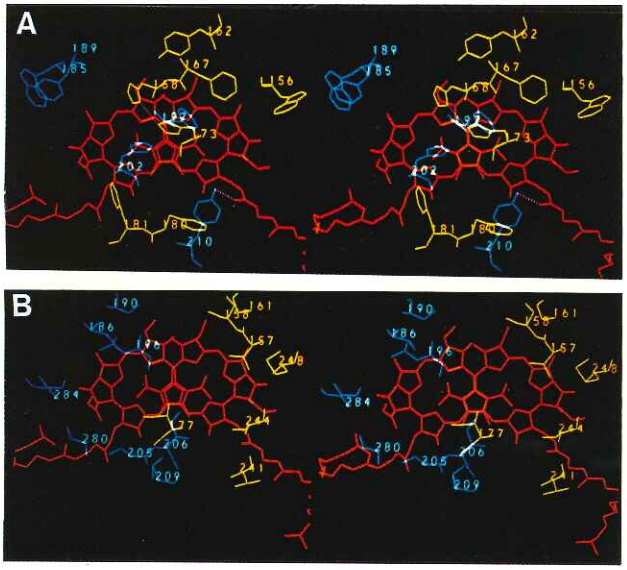

FIG. 1. Stereoplots of the Bchl dimer (red) and nearby residues (L subunit, yellow; M subunit, blue). (*A*) The aromatic residues: Phe (L167, L180, L181, M189, M197), Trp (L156, M185), Tyr (L162, M210), and His (L168, L173, and M202). (*B*) The remaining residues Gly (L161, M280), Ile (L177, M206, M284), Leu (M196, M209), Met L248, Ser (L244, M190, M205), Thr M186, and Val (L157, L241). The hydrogen bond between Tyr M210 and D_A is shown by dotted purple lines. The twofold symmetry axis is approximately aligned in the plane of the paper; the cytoplasmic side is at the bottom of the figure.

were reported to ligand to the Mg. A hydrogen bond between Ser L178 and the carbonyl oxygen of the propionic acid of ring IV of B_B is the only one between the protein subunits and the Bchl monomers. No hydrogen bond interactions involving either monomer were reported in *Rps. viridis*.

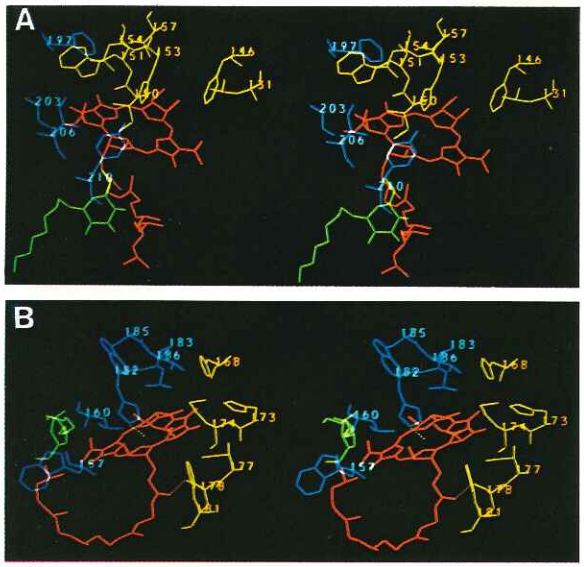

FIG. 2. Stereoplots of the Bchl monomers (red), nearby residues (L subunit, yellow; M subunit, blue), and bound detergent molecules (green). (*A*) The Bchl monomer B_A, with nearby residues Gly M203, His L153, Ile (L150, M206), Leu (L131, L154), Phe (L146, M197), Trp L151, Tyr M210, and Val L157. (*B*) The Bchl monomer B_B, the detergent βOG_B, and nearby residues His (L168, L173, M182), Ile L177, Leu (M160, M183), Met L174, Phe L181, Ser L178, Thr M186, and Trp (M157, M185). The hydrogen bond between Ser L178 and B_B is shown by a dotted purple line and the ligand between His M182 and Mg of B_B is shown by a dotted green line. The views are the same as in Fig. 1.

The Bphe. A Bphe monomer (ϕ) is found on each branch with the normal of ϕ forming an angle of 60° with respect to the membrane normal. The Bphes interact with the D and E helices as well as the B and C helices of either the L subunit (ϕ_A) or M subunit (ϕ_B) (see Fig. 3).

The only ionizable residue (other than histidines) near any of the six tetrapyrrole rings is Glu L104 near ϕ_A. Glu L104 can form a hydrogen bond to the keto carbonyl of ring V of ϕ_A and is assumed to be protonated (20, 21) (see Fig. 3). This residue is conserved in purple bacteria and was reported to be hydrogen bonded in *Rps. viridis* (8). The presence of this residue is principally responsible for the difference in the Q_x transition moments of ϕ_A and ϕ_B leading to the splitting of the absorption bands at 532 nm and 545 nm (22). The nonplanar features of the ester carbonyl group of ring V of ϕ_A (see Fig. 3) is consistent with a predominant keto form of the ring. No other possible hydrogen bonds are observed between ϕ_A and the protein subunits. However, βOG_A could possibly form a hydrogen bond to the acetyl group of ring I of ϕ_A. In *Rps. viridis*, an additional hydrogen bond was reported between the ester carbonyl group of ring V and Trp L100 (8). This residue is conserved in *Rb. sphaeroides*, but it is too far away (4.5 Å) to form a hydrogen bond.

The interactions of ϕ_B with the protein are different from those of ϕ_A (see Fig. 3*B*). The acetyl group of ring I of ϕ_B does not form a hydrogen bond with either a protein residue or βOG_B. Both the keto and ester carbonyl groups of ring V can form hydrogen bonds to Thr M133 and to Trp M129, respectively. In *Rps. viridis*, only one hydrogen bond was reported for ϕ_B between the ester carbonyl and the corresponding Trp M127 (8). Residue Thr M133 is replaced with a nonhydrogen bonding Val in *Rps. viridis*.

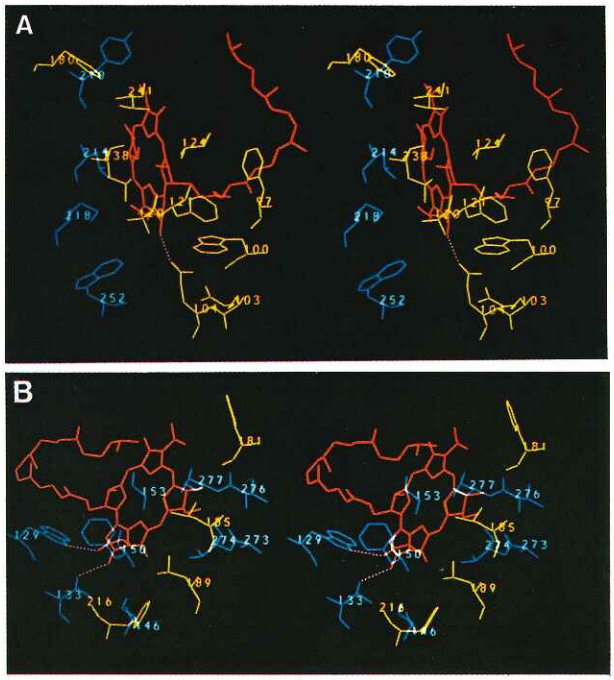

FIG. 3. Stereoplots of the Bphe (red) and nearby residues (L subunit, yellow; M subunit, blue). (*A*) The pheophytin ϕ_A, and nearby residues Ala (L120, L124), Arg L103, Glu L104, Leu (L238, M214), Met M218, Phe (L97, L121, L180), Trp (L100, M252), Tyr M210, and Val L241. (*B*) The pheophytin ϕ_B and the nearby residues Ala (M153, M273), Leu (L185, L189), Phe (L181, L216, M150), Thr (M133, M146, M277), Trp M129, and Val (M274, M276). The hydrogen bonds (between Glu L104 and ϕ_A, Trp M129 and ϕ_B, and Thr M133 and ϕ_B) are shown by dotted purple lines. The views are the same as in Fig. 1.

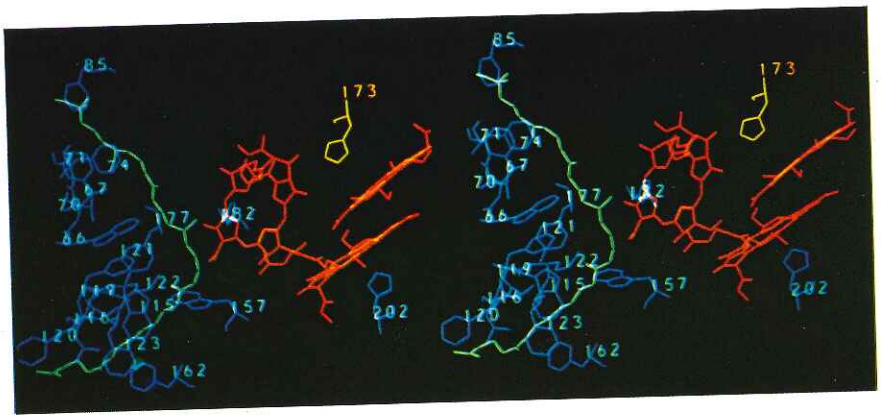

FIG. 4. Stereoplot of the carotenoid (green), the Bchl monomer B_B and the Bchl dimer D (red), and the residues (L subunit, yellow; M subunit, blue) Gly M71, His (L173, M182, M202), Ile M70, Leu M116, Met M122, Phe (M67, M74, M85, M120-121, M123, M162), Trp (M66, M115, M157), Ser M119, and Tyr M177. View is approximately down the twofold symmetry axis.

The Carotenoid. The carotenoid (C), which is spheroidene in *Rb. sphaeroides* 2.4.1, was located near the cofactor B_B between the B and C helices of the M subunit in the central hydrophobic region of the RC (see Fig. 4). The position of the carotenoid was well defined by the electron density. A 15-15′ cis bond, as identified by Raman spectroscopy (4), is consistent with the electron density, but the resolution of the structure is insufficient to position a cis bond uniquely. The nearby residues have mostly aromatic side chains that could place strong steric constraints on the conformation of the carotenoid. The constrained conformation may cause a red shift of the carotenoid's absorption spectrum relative to its spectrum in organic solvents (23). Alternatively, the shift has been modeled by assuming the presence of a few nearby charged residues (24). However, no charged residues are located at distances less than 10 Å from the carotenoid.

Bound Detergents. Two bound detergent molecules have been identified in the electron density map of RC R-26. They are denoted by βOG_A and βOG_B and are located asymmetrically relative to the twofold symmetry axis, near the Bchl monomers B_A and B_B, respectively (see Fig. 2). The position of βOG_B in RC R-26 corresponds to the position of the central region of the carotenoid in RC 2.4.1 (see *Discussion*).

DISCUSSION

Structures of Tetrapyrrole Systems. Protein–porphyrin interactions in soluble proteins may be divided into two general categories (25): (*i*) heme enzymes such as cytochrome *c* peroxidase, catalase, and cytochrome P-450 in which the heme is completely surrounded by protein and (*ii*) electron and oxygen carriers such as cytochrome *c* and globins, where one edge of the porphyrin is exposed to solvent. The interactions of Bchl and Bphe rings with the RC are similar to those observed in heme enzymes, in which these cofactors are almost completely surrounded by the protein. The amino acid residues in the Bchl and Bphe environments are predominately hydrophobic. This is in contrast with the heme enzymes (25), in which a more polar heme environment is apparently needed to stabilize the high oxidation state of iron generated during the catalytic mechanism. Structural features of this type are apparently not necessary to accommodate the charge changes of ± 1 that are distributed over the macrocycles of the Bchls and Bphes during electron transfer.

The iron atom in heme-containing proteins is either 5 or 6 coordinated with His, Tyr, Cys, and Met residues serving as protein ligands. Bchl–protein interactions have been described for the bacteriochlorophyll a protein from *Prosthecochloris aestvarii* (26) and the RC from *Rps. viridis* (8). In both cases, the chlorophyll magnesium is 5-coordinated. The bacteriochlorophyll a protein has 7 Bchl, 5 of which have the Mg coordinated to His, one Mg is coordinated to a peptide bond carbonyl oxygen, and one Mg is coordinated to a solvent molecule. In the RC from *Rps. viridis*, the Mg of all 4 Bchls are coordinated to His.

In the RC from *Rb. sphaeroides*, the Mg coordination is asymmetric; the Mgs of the B branch are 5-coordinated, while the Mgs of the A branch appear to be 4-coordinated, although the presence of a disordered water molecule as a fifth ligand cannot be excluded. This ligation asymmetry may contribute to the directional asymmetry of electron transfer as discussed below. However, it is not necessary that this ligation pattern be maintained in all oxidation states of the RC. For example, a conformation change accompanying light absorption could move His L173 closer to the Mg of D_A, which would result in a more symmetrical coordination of the dimer. Resonance Raman studies favor the symmetric 5-coordinated structure (27).

Carotenoid. Carotenoids can be incorporated into RCs from the carotenoidless strain R-26, thereby fully restoring their functional characteristics (4). Carotenoids with terminal polar functional groups were found to bind preferentially. However, no interactions are evident between the polar group of the spheroidene and the protein residues in the three-dimensional structure of RC 2.4.1. The insertion of carotenoids into RC R-26 is sensitive to detergent conditions (28) as would be expected from the observed binding of a detergent molecule in RC R-26 at the corresponding carotenoid binding site. The preferential binding of carotenoids with polar groups may also reflect interactions involving bound detergent molecules or solvent that have not yet been identified.

A possible role for B_B. The carotenoid serves, in principle, two functions: (*i*) it can transfer singlet excitation energy to the tetrapyrroles in an analogous manner to the antenna pigments (its likely role during the early stage of evolution) and (*ii*) it reduces the lifetime of the triplet state of the dimer by 3 orders of magnitude (4), thereby protecting the RC against photooxidation damage. The closest approach of C to D is too large (10.5 Å to ring V of D_B) for efficient energy transfer. The observed efficient energy transfer of the triplet state from D to C is believed to be facilitated by B_B, which bridges D and C; the closest approach of B_B to both C and D is $\approx$4 Å. The involvement of a Bchl monomer in the triplet transfer had been suggested from spectroscopic measurements (29). Thus, B_B participates in *energy transfer* along the "inactive" B branch, whereas B_A participates in *electron transfer* along the "active" A branch.

Removal of B_B. The Bchl monomer B_B can be removed with borohydrate (30). This removal may be associated with

the presence of the nearby detergent molecule. The bulk of βOG_B lies within 7 Å of B_B and has a closest approach to B_B and His M182 of 3.5 Å and 4.5 Å, respectively (Fig. 2*A*). In contrast, only one edge of the ring of βOG_A lies within 7 Å of B_A and the closest approach of βOG_A to His L153 is 7.5 Å (Fig. 2*B*). The close proximity of βOG_B to B_B suggests that B_B is more accessible to solvent than B_A. This is consistent with the preferential removal of B_B from RCs isolated from strain R-26. In the wild-type strain, the removal of B_B is accompanied by the removal of the carotenoid (31).

The Primary Electron Transfer Rate. After photoexcitation of the dimer, an electron is transferred to ϕ_A in ≈3 ps (32). There are two main questions concerning this process: (*i*) what is the mechanism responsible for such a fast transfer rate and (*ii*) what causes the preferential electron transfer along the A branch? An examination of the three-dimensional structure suggests some answers to these questions.

The distance of closest approach between the tetrapyrrole rings of D and ϕ_A is 10 Å. It is difficult to account for the 3-ps transfer time over such a large distance. Consequently, the involvement of the bridging monomer, B_A, has been invoked to account for the observed transfer rate (33–36). In addition, two other bridging mechanisms may play a role in the electron transfer. First, the phytyl chain of D_A makes van der Waals contacts with ϕ_A; electron conduction along the hydrocarbon chain may be possible. Second, Tyr M210 lies ≈4.5 Å from D and ϕ_A and may play a role in the electron transfer in purple photosynthetic bacteria, although this residue is not conserved in green bacteria or plant systems.

It has been found experimentally that electron transfer proceeds preferentially along the A branch (for a review, see ref. 37). This asymmetry in the electron transfer rate can be accounted for by the breaking of the twofold symmetry at different places of the reaction center: (*i*) there is an inherent asymmetry in the dimer structure because of different nonplanar features of the tetrapyrroles, Mg coordination, and hydrogen bonding of the two halves, D_A and D_B. (*ii*) The overlap between D_B and B_A is larger than the corresponding overlap between D_A and B_B (2). (*iii*) The Bphe, ϕ_A, is 1–1.5 Å closer to both B_A and Tyr M210 than ϕ_B is to B_B and Phe L181, respectively. (*iv*) The distribution of charged amino acids is asymmetric (6). The effect on the electron-transfer rate of structural asymmetries has been calculated by Plato *et al.* (38) for *Rps. viridis*; the ratio of rates along the A and B paths was found to be 34, which is consistent with the experimentally determined limit of >20 (37). Studies on site-specific mutants should shed further light on the importance of these structural asymmetries.

We thank E. Abresch for the preparation of the RCs and M. Y. Okamura and W. Lubitz for helpful discussions. This work was supported by grants from the National Institutes of Health (AM36053, GM13191, GM31875), the National Science Foundation (DMB85-18922), and a Presidential Young Investigators Award. D.C.R. is an A. P. Sloan research fellow.

1. Okamura, M. Y., Feher, G. & Nelson, N. (1982) in *Photosynthesis*, ed. Govindjee (Academic, New York), pp. 195–272.
2. Allen, J. P., Feher, G., Yeates, T. O., Komiya, H. & Rees, D. C. (1988) in *The Photosynthetic Bacterial Reaction Center*, eds. Breton, J. & Vermeglio, A. (Plenum, New York), pp. 5–11.
3. Allen, J. P., Feher, G., Yeates, T. O., Komiya, H. & Rees, D. C. (1987) *Proc. Natl. Acad. Sci. USA* **84,** 5730–5734.
4. Cogdell, R. J. & Frank, H. A. (1988) *Biochim. Biophys. Acta* 895, 63–79.
5. Allen, J. P., Feher, G., Yeates, T. O., Komiya, H. & Rees, D. C. (1987) *Proc. Natl. Acad. Sci. USA* **84,** 6162–6166.
6. Yeates, T. O., Komiya, H., Rees, D. C., Allen, J. P. & Feher, G. (1987) *Proc. Natl. Acad. Sci. USA* **84,** 6438–6442.
7. Allen, J. P., Feher, G., Yeates, T. O., Komiya, H. & Rees, D. C. (1988) *Proc. Natl. Acad. Sci. USA*, in press.
8. Michel, H., Epp, O. & Deisenhofer, J. (1986) *EMBO J.* **5,** 2445–2451.
9. Tiede, D. M., Budil, D. E., Tang, J., El Kabbani, O., Norris, J. R., Chang, C. H. & Schiffer, M. (1988) in *The Photosynthetic Bacterial Reaction Center*, eds. Breton, J. & Vermeglio, A. (Plenum, New York), pp. 13–20.
10. Artymiuk, P. J. & Blake, C. C. F. (1981) *J. Mol. Biol.* **152,** 737–762.
11. Hendrickson, W. A. (1985) *Methods Enzymol.* **115,** 252–270.
12. Read, R. J. (1986) *Acta Crystallogr. Sect. A* **42,** 140–149.
13. Hamlin, R. (1985) *Methods Enzymol.* **114,** 416–452.
14. Reeke, G. N. (1984) *J. Appl. Crystallogr.* **17,** 125–130.
15. Yeates, T. O. & Rees, D. C. (1988) *J. Appl. Crystallogr.*, in press.
16. Deisenhofer, J., Epp, O., Miki, K., Huber, R. & Michel, H. (1984) *J. Mol. Biol.* **180,** 385–398.
17. Thompson, M. A. & Zerner, M. C. (1988) *J. Am. Chem. Soc.* **110,** 606–607.
18. Deisenhofer, J. & Michel, H. (1988) in *The Photosynthetic Bacterial Reaction Center*, eds. Breton, J. & Vermeglio, A. (Plenum, New York), pp. 1–3.
19. Komiya, H., Yeates, T. O., Rees, D. C., Allen, J. P. & Feher, G. (1988) *Proc. Natl. Acad. Sci. USA*, in press.
20. Feher, G., Isaacson, R. A., Okamura, M. Y. & Lubitz, W. (1988) in *The Photosynthetic Bacterial Reaction Center*, eds. Breton, J. & Vermeglio, A. (Plenum, New York), pp. 229–235.
21. Nabedryk, E., Andrianambinintsoa, S., Mäntele, W. & Breton, J. (1988) in *The Photosynthetic Bacterial Reaction Center*, eds. Breton, J. & Vermeglio, A. (Plenum, New York), pp. 237–250.
22. Bylina, E. J., Kirmaier, C., McDowell, L., Holten, D. & Youvan, D. C. (1988) *Nature (London)*, in press.
23. Frank, H. A., Chadwick, B. W., Taremi, S., Kolaczkowski, S. & Bowman, M. K. (1986) *FEBS Lett.* **203,** 157–163.
24. Kakitani, T., Honig, B. & Crofts, A. R. (1982) *Biophys. J.* **39,** 57–63.
25. Poulos, T. L. (1987) *Adv. Inorg. Biochem.* **7,** 1–36.
26. Tronrud, D. E., Schmid, M. F. & Matthews, B. W. (1986) *J. Mol. Biol.* **188,** 443–454.
27. Zhou, Q., Robert, B. & Lutz, M. (1987) *Biochim. Biophys. Acta* **890,** 368–376.
28. Agalidis, I., Lutz, M. & Reiss Husson, F. (1980) *Biochim. Biophys. Acta* **589,** 264–274.
29. Schenck, C. C., Mathis, P. & Lutz, M. (1984) *Photochem. Photobiol.* **39,** 407–417.
30. Ditson, S. L., Davis, R. C. & Pearlstein, R. M. (1984) *Biochim. Biophys. Acta* **766,** 623–629.
31. Frank, H. A., Taremi, S. S., Knox, J. R. & Mäntele, W. (1988) in *The Photosynthetic Bacterial Reaction Center*, eds. Breton, J. & Vermeglio, A. (Plenum, New York), pp. 27–32.
32. Kirmaier, C. & Holten, D. (1987) *Photosynth. Res.* **13,** 225–260.
33. Marcus, R. A. (1987) *Chem. Phys. Lett.* **133,** 471–477.
34. Bixon, M., Jortner, J., Michel-Beyerle, M. E., Ogrodnik, A. & Lersch, W. (1987) *Chem. Phys. Lett.* **140,** 626–630.
35. Fischer, S. F. & Scherer, P. O. J. (1987) *Chem. Phys.* **115,** 151–158.
36. Creighton, S., Hwang, J. K., Warshel, A., Parson, W. W. & Norris, J. (1988) *Biochemistry* **27,** 774–781.
37. Michel-Beyerle, M. E., Plato, M., Deisenhofer, J., Michel, H., Bixon, M. & Jortner, J. (1988) *Biochim. Biophys. Acta* **932,** 52–70.
38. Plato, M., Lendzian, F., Lubitz, W., Tränkle, E. & Möbius, K. (1988) in *The Photosynthetic Bacterial Reaction Center*, eds. Breton, J. & Vermeglio, A. (Plenum, New York), pp. 379–388.